Monthly Notices
of the
ROYAL ASTRONOMICAL SOCIETY

Mon. Not. R. Astron. Soc. **402,** 1667–1674 (2010) doi:10.1111/j.1365-2966.2009.16053.x

Large prebiotic molecules in space: photophysics of acetic acid and its isomers

Fabrizio Puletti,[1] Giuliano Malloci,[2] Giacomo Mulas[2] and Cesare Cecchi-Pestellini[2]★

[1]*Dipartimento di Fisica, Universitá di Cagliari, Strada Prov. le Monserrato-Sestu Km 0.700, I-09042 Monserrato (CA), Italy*
[2]*INAF – Osservatorio Astronomico di Cagliari, St. 54 Loc. Poggio dei Pini, I-09012 Capoterra (CA), Italy*

Accepted 2009 November 16. Received 2009 November 9; in original form 2009 July 20

ABSTRACT

An increasing number of large molecules have been positively identified in space. Many of these molecules are of biological interest and thus provide insight into prebiotic organic chemistry in the protoplanetary nebula. Among these molecules, acetic acid is of particular importance due to its structural proximity to glycine, the simplest amino acid. We compute electronic and vibrational properties of acetic acid and its isomers, methyl formate and glycolaldehyde, using density functional theory. From the computed photoabsorption cross-sections, we obtain the corresponding photoabsorption rates for solar radiation at 1 au and find them in good agreement with previous estimates. We also discuss glycolaldehyde diffuse emission in Sgr B2(N), as opposite to emissions from methyl formate and acetic acid that appear to be concentrated in the compact region Sgr B2(N-LMH).

Key words: astrochemistry – molecular processes – methods: numerical.

1 INTRODUCTION

The richness of interstellar chemistry has been growing steadily with a variety of objects and regions observed. The excitation and abundances of molecules contain key information on the physical structure and evolution of the host regions. Through molecules, we can trace the cycle of matter for interstellar space into stars and planets and back again into the interstellar space (Hartquist & Williams 1998).

There is an increasing body of evidence for the existence of large molecules in the interstellar medium and in the interplanetary space. Interferometric observations of high-mass star-forming regions in molecular clouds have revealed hot molecular cores, short-lived remnants of clouds not incorporated into the newly born massive stars. These hot cores contain within them the evaporated material of ices deposited on dust grain surfaces during the collapse, and observations show a very interesting chemistry. In particular, there exist substantial column densities of large partly hydrogen-saturated molecules, many of them being of prebiotic interest. Some of these species have also been observed in comets and embedded in minor bodies of the Solar system (Chyba & Hand 2005). The study of biologically interesting large interstellar molecules offers the exciting opportunity of learning more about the chemical evolution preceding the onset of life on the early Earth 4.5 billion years ago. Comets may be important carriers of prebiotic chemistry and relevant agents in the delivery of complex organics to the early Earth as well as to newly formed planets.

★E-mail: ccp@ca.astro.it

The Sgr B2 molecular cloud complex is the prime target in the search for complex species, in particular in a hot core, the so-called Large Molecule Heimat, Sgr B2(N-LMH), within the more extended molecular cloud. In this compact source, smaller than the Oort cloud ($\sim$0.08 pc) with a mass of several thousand $M_\odot$ (Miao & Snyder 1997), an extraordinary number of complex organics have been observed to exhibit very high column densities (e.g. amino acetonitrile; Belloche et al. 2008). Large partly hydrogen-saturated species challenge the completeness of the standard ion-neutral scheme in interstellar chemistry, suggesting that reactions on dust grains are involved in their formation (e.g. Bennett & Kaiser 2007).

Of the chemical species detected so far, particular attention has been paid to the formation of different isomer groups. In this work, we focus on $C_2H_4O_2$, i.e. acetic acid (CH_3COOH), glycolaldehyde ($HCOCH_2OH$) and methyl formate ($HCOOCH_3$), because of their potential role in the origin of life (e.g. Wächtershäuser 2000; Chyba & Hand 2005). Glycolaldehyde, the simplest of the monosaccharide sugars, has first been detected by Hollis, Lovas & Jewell (2000) towards Sgr B2(N-LMH), and its most recently determined column density in that source is 5.9×10^{13} cm^{-2} (Halfen et al. 2006). It has been recently observed outside the Galactic Centre by Beltrán et al. (2009) towards the hot molecular core G31.41+0.31, with the emission coming from the hot and dense region closest to the protostars. In addition, Crovisier et al. (2004) and Despois et al. (2005) presented an upper limit for glycolaldehyde abundance in the comet Hale-Bopp. Acetic acid shares the C−C−O backbone with glycine, from which it differs by an amino group (NH_2). First detected by Mehringer et al. (1997) in Sgr B2(N-LMH), acetic acid shows a column density of 6.1×10^{15} cm^{-2} in that region (Remijan et al. 2002). Finally, methyl formate, discovered towards Sgr B2(N)

by Brown et al. (1975), has been also observed in other star-forming regions of both high (MacDonald et al. 1996; Gibb et al. 2000) and low (Remijan & Hollis 2006) mass, towards a protoplanetary nebula (Remijan et al. 2005), and in comets (Bockelée-Morvan et al. 2000; Despois et al. 2005; Remijan et al. 2006). The column density of methyl formate in Sgr B2(N-LMH) is $1.1 \times 10^{17}\,\mathrm{cm}^{-2}$ (Liu, Mehringer & Snyder 2001).

Sgr B2(N-LMH) is the only source where all three of these isomers have been observed. However, while acetic acid and methyl formate are concentrated in Sgr B2(N-LMH), glycolaldehyde appears to be more diffusely spread through Sgr B2(N) (Hollis et al. 2001). This behaviour is generally shared by other aldehydes (Snyder 2006). In comets, only methyl formate has been observed so far.

An understanding of molecular structure, spectroscopy and photoabsorption processes may be of critical importance in interpreting current observations. In particular, the lifetime of cometary molecules versus photodestruction is a basic parameter for all cometary studies: as a matter of fact any error in the photodissociation rate translates linearly into an error on the abundance derived in the cometary nucleus. It is also needed for chemical modelling of planetary atmospheres. In this work, we derive electronic and vibrational properties of the isomer triplet $C_2H_4O_2$ described above using the density functional theory (DFT). Photodestruction rates for acetic acid and methyl formate were derived by Crovisier (1994) using old laboratory absorption data published by Suto, Wang & Lee (1988), while the rate for glycolaldehyde is just an estimate. In Section 2, we present a brief outline of the method, together with a description of computational settings and results. Section 3 contains the application of these results to cometary photochemistry, while discussion and conclusions are given in Section 4.

2 THEORY AND RESULTS

We used DFT (e.g. Jones & Gunnarsson 1989) for the calculation of the equilibrium geometry of the electronic ground state and of the vibrational spectrum. We then applied the time-dependent extension of the theory (TD-DFT; Marques & Gross 2004) to compute the electronic excited states and the resulting photoabsorption spectrum for each molecule.

To obtain the ground-state optimized geometries, we used the quantum chemistry program package TURBOMOLE (Ahlrichs et al. 2007). Technical details about the specific choice of density functional and atomic basis set can be found in the Appendix.

After geometry optimization, we performed the vibrational analysis obtaining energies and intensities of the normal modes of vibration in the harmonic approximation. Vibrational transitions for fundamental configurations of the isomer triplet are given in the Appendix.

Finally, keeping fixed the ground-state geometries obtained above, we computed the photoabsorption cross-section for each molecule. We used two different implementations of TD-DFT in the linear response regime, in conjunction with different representations of the Kohn–Sham wavefunctions:

(i) the real-time propagation scheme using a grid in real space (Yabana & Bertsch 1999), as implemented in the OCTOPUS computer program (Marques et al. 2003);

(ii) the frequency-space implementation (Bauerschmitt & Alrichs 1996) based on the linear combination of localized orbitals, as given in TURBOMOLE.

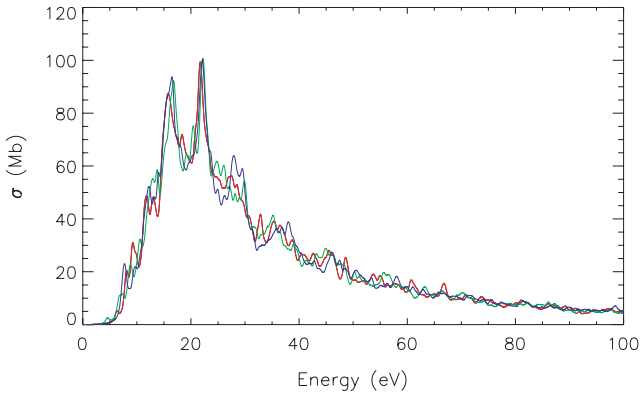

Figure 1. Comparison between the photoabsorption cross-sections (in Megabarns, $1\,\mathrm{Mb} = 10^{-18}\,\mathrm{cm}^2$) of acetic acid (red), methyl formate (blue) and glycolaldehyde (green), as computed up to 100 eV using the real-time TD-DFT implementation in the OCTOPUS program.

In the real-time propagation scheme (i) the whole photoabsorption cross-section of the molecule, up to the far-UV, is obtained at once, which is particularly convenient for astrophysical applications. Technical details about the TD-DFT formalism implemented in the OCTOPUS program are reported in the Appendix; the resulting spectra are displayed in Fig. 1.

In the most widely used frequency-space implementation (ii) the poles of the linear response function correspond to vertical excitation energies and the pole strengths to the corresponding oscillator strengths. With this method, computational costs scale steeply with the number of required transitions; electronic excitations are thus usually limited to the low-energy part of the spectrum. Table 1 shows that both combinations BP-TZVP and B3LYP-TZVP (see the Appendix for the nomenclature) provide a similarly good agreement between the computed transitions and the experimental results available for acetic acid at room temperature (Limão-Vieira et al. 2006), while BP-TZVP results in a much closer agreement with the experimental results for glycolaldehyde (Karunanandan

Table 1. Comparison between the computed electronic transitions as obtained using different exchange–correlation functionals and the experimental data reported by Limão-Vieira et al. (2006) for acetic acid and by Karunanandan et al. (2007) for glycolaldehyde.

BP/TZVP	B3LYP/TZVP	EXP
	Acetic acid	
5.60	5.84	6.09
6.93	7.49	7.22
8.20	8.30	8.15
8.25	8.50	8.35
9.20	9.25	8.82
10.07	10.54	10.29
	Average relative error (per cent)	
3.4	3.2	
	Glycolaldehyde	
4.49	5.61	4.51
	Average relative error (per cent)	
0.4	24.4	

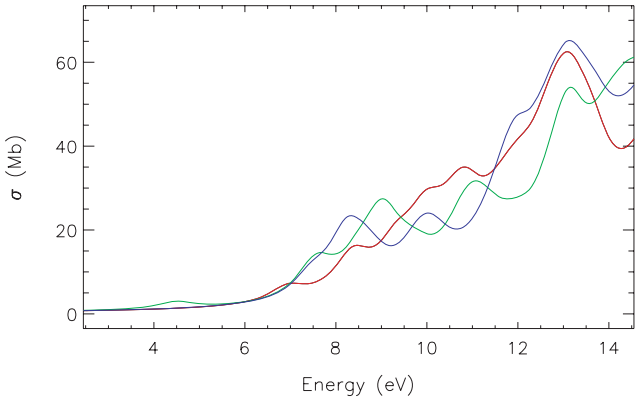

Figure 2. Same as Fig. 1 as obtained for the low-energy part of the spectrum using the frequency-space TD-DFT implementation of the TURBOMOLE package at the BP/TZVP level of theory.

et al. 2007). We therefore chose to use the BP functional for all of our calculations. The resulting BP-TZVP absorption spectra for the three molecules, shown in Fig. 2, are obtained as a superposition of Gaussian functions with fixed arbitrary widths of 0.8 eV. The kind of calculations we performed only yield the positions and intensities of vertical, pure electronic transitions and therefore give no information on band widths. However, in the available gas-phase spectra of acetic acid (Limão-Vieira et al. 2006) and glycolaldehyde (Karunanandan et al. 2007), bands up to ∼10 eV show broad profiles with a full width at half-maximum (FWHM) of about 0.8 eV, produced by the convolution of unresolved vibronic structure and the natural width of the transitions. The list of first 50 excited states and transition intensities is given in Table A1.

The two TD-DFT implementations produce compatible results in the low-energy region, i.e. up to about 10 eV, while they tend to diverge significantly at higher energies. However, TD-DFT, as a method, is known to yield dependable results for individual transitions only for excitation energies up to the ionization energy, which indeed is close to ∼10 eV for all three isomers.

The real-time real-space implementation, on the other hand, has been demonstrated to yield good results for the overall density of electronic transitions even at high energies, with the *caveat* that single peaks of fine structure are meaningless (see e.g. Marques et al. 2003): at energies of $\gtrsim$10 eV only the *envelope* of the spectra calculated by OCTOPUS is expected to be accurate, while the resolved fine structure is largely due to standing waves in the finite simulation box, is strongly dependent on the size of the box and is only partly quenched by the absorbing boundary conditions we adopted. Since we use these spectra at high energies to compute absorption rates in a continuous spectrum (see Section 3), the effect of spurious fine structure averages out when integrating over ranges of many eVs, making these theoretical spectra quite adequate for their intended purpose.

3 PHOTOCHEMISTRY

The photoabsorption rates of the three isomers are computed by means of the relation

$$\beta\,(\mathrm{s}^{-1}) = \int_{\Delta E} S_{\odot}(E)\sigma(E)\mathrm{d}E, \qquad (1)$$

where, for the sake of comparison, $S_{\odot}(E)$ is the solar spectrum at 1 au provided by Huebner, Keady & Lyon (1992) and $\sigma(E)$ the photoabsorption cross-section for a given molecule. The resulting photoabsorption rates are reported in Table 2, where we also show results for a radiation density expected in a photodissociation front near an OB star (Draine & Bertoldi 1996). We also list separately the contribution of the Lyα line in the solar spectrum to the absorption rates, which is of the order of ∼15 per cent of the total, in agreement with previous estimates of Crovisier (1994). As evident in Fig. 2 and Table A1 , glycolaldehyde presents a relatively strong band near 4.5 eV, at an energy of ∼2 eV lower than the first transitions of comparable intensity in the other two members of the triplet (namely ∼6.9 eV for acetic acid and ∼7.5 eV for methyl formate). Since the solar spectral distribution decreases very steeply in this energy range, the estimated glycolaldehyde photoabsorption rate in the solar radiation field is by and large dominated by this single band and results to be more than 100 times larger than those of acetic acid and methyl formate. This effect is not present for photoabsorption rates estimated for the Draine & Bertoldi (1996) spectrum, since it is much flatter than the solar one in the UV, and thus no single band dominates the absorption for any of the three species. TD-DFT calculations are known to provide transition energies accurate within about 0.3 eV. To test the robustness of our results, we shifted the energies of all transitions by ±0.3 eV and checked how this affects the resulting photoabsorption rates. Also, since TD-DFT provides no information on the intrinsic width of the calculated bands, we assumed for all bands an FWHM of ∼0.8 eV, consistent with published experimental data (Limão-Vieira et al. 2006; Karunanandan et al. 2007). The overall variations in photoabsorption rates are within a factor of 2, meaning that our conclusions are rather firm. This accuracy may appear surprising for the estimated absorption rates in the Lyα line, which would naively be expected to vary very strongly with the calculated positions of molecular bands, producing either a very large absorption rate if it happens to be close to a strong one or a very small one if it falls in a gap in the absorption spectrum; however, the assumption (based on experimental data) of a 0.8 eV FWHM for all bands vastly reduces the dependence of absorption rates on small (i.e. ∼0.3 eV) variations in band positions.

In a recent analysis of ice composition in comet Hale-Bopp, Crovisier et al. (2004) quote a photodestruction rate (at 1 au) for acetic acid $\beta_{\mathrm{CH_3COOH}} = 5.1 \times 10^{-5}\,\mathrm{s}^{-1}$. This value was provided by Crovisier (1994), who also reported a rate $\beta_{\mathrm{CH_3OHCO}} = 4.7 \times 10^{-5}\,\mathrm{s}^{-1}$ for methyl formate. The photodestruction rate of glycolaldehyde is unknown and assumed to be $1 \times 10^{-4}\,\mathrm{s}^{-1}$ at 1 au (Crovisier et al. 2004). Assuming a unit photodestruction yield and a factor of 2 indetermination in the calculations, our photodestruction rates are consistent with Crovisier (1994) values, which were based on old laboratory data provided by Suto et al. (1988). The case of glycolaldehyde is different, since most of photoabsorption is produced by the band at 4.5 eV, that appears to be too low in energy to provide a unit photodestruction yield. As a consequence, photodestruction channels are activated just via absorption in the high-energy bands, leading to a photoabsorption rate $\beta^{\star}_{\mathrm{CH_2OHCHO}} \sim 3 \times 10^{-5}\,\mathrm{s}^{-1}$ (cf. Table 2), much lower than the rate assumed in Crovisier et al. (2004).

Photons absorbed in the lower energy bands of CH_2OHCHO may be resonantly scattered or, if the molecule undergoes internal conversion, re-emitted in the IR range. Using an adapted version of a Monte Carlo model developed for emission by polycyclic aromatic hydrocarbons, which is indeed assumed to be pumped by complete internal conversion of the energy absorbed via electronic transitions in the visible and UV (Mulas 1998), we have constructed the expected IR emission by glycolaldehyde, powered by the solar flux at 1 au, assuming all the energy absorbed in the band at ∼4.5 eV to be emitted in the IR. The emission coefficient (per molecule) is reported in Fig. 3.

Table 2. Photoabsorption rates (s^{-1}) for the isomer triplet $C_2H_4O_2$ in two radiation fields, assuming a band FWHM of ∼0.8 eV based on available experimental data (Limão-Vieira et al. 2006; Karunanandan et al. 2007).

Species		Solar flux at 1 au (Huebner et al. 1992)	Solar Lyα at 1 au (Huebner et al. 1992)	Unshielded OB field (Draine & Bertoldi 1996)
Acetic acid	CH_3COOH	6.7(−5)[a]	9.7(−6)	2.9(−9)
Glycolaldehyde[b]	$HCOCH_2OH$	9.6(−3)	–	1.3(−10)
		2.8(−5)	3.7(−6)	2.9(−9)
Methyl formate	$HCOOCH_3$	5.0(−5)	7.4(−6)	3.0(−9)

Note. The first column lists the computed absorption rates for the whole solar spectrum at 1 au (Huebner et al. 1992), the second column in the solar Lyα line at 1 au (Huebner et al. 1992) and the third in a photodissociation front near an OB star (Draine & Bertoldi 1996).
[a]$1.8(-5) = 1.8 \times 10^{-5}$.
[b]First row: photoabsorption rates due to the first two absorption bands (up to ∼4.5 eV); second row: photoabsorption rates due to the remaining bands.

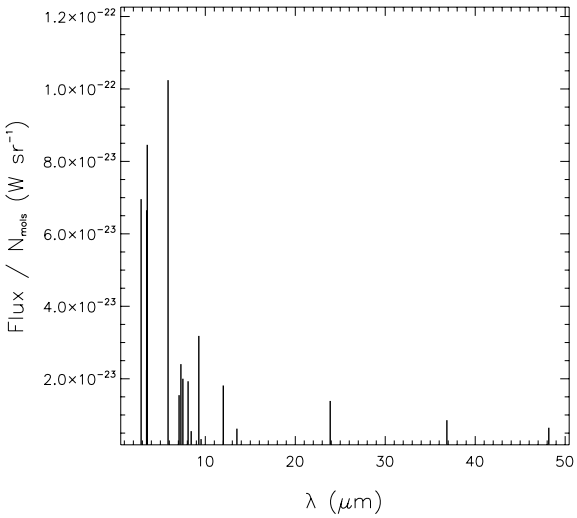

Figure 3. IR emission spectrum of one glycolaldehyde molecule at 1 au from the quiet Sun, estimated by assuming that all the energy absorbed in electronic transitions is converted in vibrational excitation and subsequently reradiated (see text). Emission in each vibrational band is represented by a vertical bar whose abscissa corresponds to the wavelength of the vibrational mode and whose height equals the calculated emission intensity.

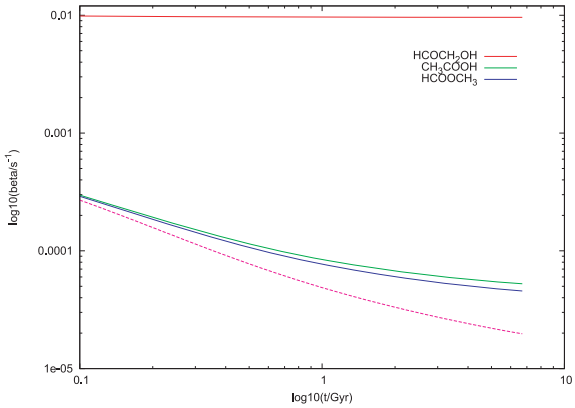

Figure 4. Photoabsorption rates in the environments of solar-type stars of different ages. Top to bottom: glycolaldehyde, acetic acid, methyl formate and glycolaldehyde with the band at 4.5 eV suppressed.

We have thus far considered photoabsorption rates in the standard solar radiation field at 1 au (for the 'quiet' Sun), which are relevant for the photochemistry of glycolaldehyde, acetic acid and methyl formate in our present Solar system. However, from the study of stellar proxies for the Sun, it appears that young solar-type stars emit high-energy photons at a level three to four orders of magnitude higher than the present-day Sun, both during the pre-main-sequence phase when the emission is dominated by intense daily or weekly flares (Favata et al. 2005) and during the first phases of the main sequence (Micela 2002). Therefore, chemical evolution can only be understood within the context of the evolving stellar radiation environment.

Without addressing the problem of molecular survival in a disc (e.g. Visser et al. 2007), we estimate the effect of the extreme UV emission (roughly the spectral range between 13 and 100 eV) from solar-type stars of different ages, exploiting the emission of six stars from the Sun in TIME program (Guinan & Ribas 2002), whose fluxes are assumed to describe the evolution of the Sun's emission (Ribas et al. 2005). Since Ribas et al. (2005) reported integrated fluxes (at 1 au), the rate coefficients are approximated by

$$\beta(t)\,(\mathrm{s}^{-1}) = \sum_{\Delta E} \langle\sigma\rangle_{\Delta E}\ \frac{S_{\odot}(t, \Delta E)}{\Delta E}, \qquad (2)$$

where $\langle\sigma\rangle_{\Delta E}$ is the average over the energy range ΔE of the photoabsorption cross-sections shown in Fig. 1. ΔE intervals are taken from Ribas et al. (2005), Table A1. Beyond 100 eV, a collective description of the molecule is no longer necessary, since X-ray absorption cross-sections can be closely approximated by adding the atomic cross-sections of individual atoms bound in the molecule (e.g. Cecchi-Pestellini, Ciaravella & Micela 2006). We therefore do not perform calculations in the X-ray energy range here. Results are reported in Fig. 4. It is evident that the high-energy tail of stellar spectrum provides a significant enhancing of photoabsorption rates for acetic acid and methyl formate. Glycolaldehyde photon absorption rates are not changing too much, although the extreme UV contribution to photoabsorption is comparable to absorption in the near-UV band at ∼4.5 eV. In general, due to the increase in the stellar high-energy component, the photodestruction rates of the isomer triplet members increase roughly by two orders of magnitude in the environment of a young solar-like star.

4 DISCUSSION AND CONCLUSIONS

In this work, we studied the photophysics of the acetic acid and its isomers, glycolaldehyde and methyl formate. Computed photoabsorption rates are consistent with the literature data for acetic acid

and methyl formate. In the case of glycolaldehyde, for which the photoabsorption was completely missing up to the far-UV, our calculations indicate that photodestruction is slower than in the other two members of the isomer triplet. However, the overall photoabsorption rate is much larger and likely to produce either resonant scattering or IR emission powered by near-UV solar photons.

Sgr B2 observations of glycolaldehyde show that, unlike acetic acid and methyl formate, its emission is extended in the surrounding molecular cloud. Such a behaviour, which has not been understood so far (e.g. Chengalur & Kanekar 2003), is part of a more general problem involving differentiation in isomers, such as isocyanide isomers (CH_3CN, CH_3NC). The behaviour of this isomer triplet has also recently been discussed by Lattelais et al. (2009) as a notable exception to what was called the 'minimum energy principle' (MEP) whereby whenever several isomers are possible for a given formula, their observed abundances are in order of binding energy. The authors made the educated guess that this anomaly is first created by differences in the chemical pathways leading to the formation of glycolaldehyde, acetic acid and methyl formate on the surfaces of dust grains, and then preserved due to large energy barriers for the conversion among them. Our results may help us to shed some more light on this problem. Although both hot core and the embedding molecular cloud are dark regions, cosmic rays provide a source of UV photons at high visual extinctions by exciting molecular hydrogen in the Lyman and Werner bands (Prasad & Tarafdar 1983). This locally generated photon flux typically has fluences lower than 10 000 photons cm^{-2} s^{-1} (Cecchi-Pestellini & Aiello 1992) and may produce important chemical effects (Gredel et al. 1989; Bennett & Kaiser 2007). However, the similarity in both the photoabsorption cross-sections and ionization potentials of the three species makes chemical differentiation due to selective photodestruction unlikely. As a possible explanation of the extended spatial scale of glycolaldehyde, we consider the possibility of a slow, selective isomerization, i.e. the possibility that a species may convert itself into another member of the $C_2H_4O_2$ triplet by interacting with the radiation field. This would imply an isomerization mechanism which operates on a time-scale which is much longer than the typical lifetime of a hot core (few times 10^4 years; Wilner et al. 2001) but still short enough to be effective on the time-scale of the lifetime of a molecular cloud ($\sim 10^8$ years; Williams, Blitz & McKee 2000). In this framework, hot cores would reflect the relative abundances among the isomers as created by their production mechanisms, whereas in the molecular cloud the isomers would 'relax' to the most stable one, namely glycolaldehyde, in agreement with the MEP.

Isomerization may be induced by the absorption of radiation essentially in two main ways; following the absorption of a UV-visible photon, the molecule could

(i) move to an electronic state whose energy surface presents a minimum close to the equilibrium configuration of another isomer;
(ii) convert, via one or more non-radiative transitions, a substantial part of the electronic excitation energy into vibrational energy allowing the overcoming of the isomerization potential barriers.

The present data do not allow a discrimination between the two cases. Moreover, the analysis of the first isomerization channel would require a detailed study of the energy hypersurfaces in the excited states accessible with photons generated by the Prasad & Tarafdar (1983) mechanism. Therefore, we will discuss qualitatively the second isomerization process. We assume that every absorption heats up the molecule in a time-scale characteristic of electronic transitions ($\sim 10^{-8}$ s), which then decays via non-radiative transitions ($\lesssim 10^{-10}$ s). The electronic excitation energy can be uniquely released by a cascade of vibrational transitions. We also assume, as simplifying hypotheses, that (i) all the excitation energy is converted in vibrational excitation, (ii) there exist only one isomerization barrier, (iii) the excitation energy is far greater than this barrier and (iv) the isomerization rate is high above the threshold and zero below it. Then every time a molecule absorbs a UV-visible photon, it will be vibrationally heated. If the energy of the absorbed photon is above the isomerization threshold, the molecule will establish a statistical equilibrium, in which the probability of finding it in one of the isomeric configurations will be proportional to the density of vibrational states at the given energy. The molecule will then cool down, in time-scales of the order of a second, with a vibrational cascade (all vibrational modes are IR-active for all three isomers). Its energy will thus eventually fall below the barrier for the isomerization. When this happens, the proportion among the isomers is frozen because the conversion rate among the species drops to zero; the abundances are therefore those given by the ratios among the densities of vibrational states. Since we are here dealing with three conformations, one should consider at least three different isomerization channels, each with its different barrier(s). Whatever they are, however, as long as they are easily overcome with the energy of a single UV photon, the ratio of the abundances of the isomers, if they are exposed to UV light, should be fixed at the ratios of the densities of states at the threshold(s).

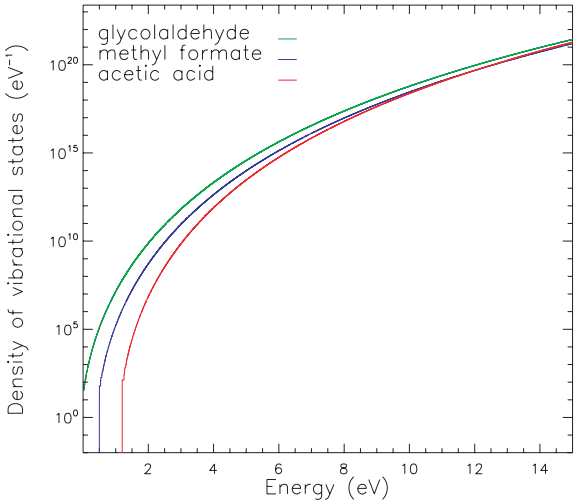

Figure 5. Densities of the vibrational states for the three species as a function of energy.

Table 3. Total energies for the three species considered.

	Total energy (eV)	δ(eV)
Glycolaldehyde	−6231.83	–
Metyl formate	−6232.32	0.49
Acetic acid	−6233.04	1.21

Note. The second column shows the energy difference δ in comparison with glycolaldehyde.

The densities of vibrational states for the three species, calculated in harmonic approximation through the algorithm of Stein & Rabinovitch (1973), are shown in Fig. 5. The distances among the curves are due to the differences in the total energies shown in Table 3 and the differences in the frequencies of the vibrational modes.

The naive model drawn above would essentially turn all isomers into glycolaldehyde as soon as they absorb a UV photon. However, UV absorption, produced by cosmic-ray-induced H_2 fluorescence in the weak radiation field, occurs on time-scales of the order of $\gtrsim$50 000 years, that are comparable to the lifetime of hot cores. As consequence, MEP should not operate effectively in the hot core phase.

Therefore, one of the simplistic assumptions in the naive model must be incorrect, slowing down isomerization. Either internal conversion has a low quantum yield for these molecules, meaning that they get vibrationally heated only a small fraction of the times they absorb a UV photon, or isomerization is *not* fast whenever vibrational excitation is sufficient to overcome reaction barriers, due to the morphology of the molecular potential energy surface. The latter can easily be the case if the unimolecular reaction path(s) to isomerization is narrow and complicated in terms of phase space of the ions.

Of course, conversion among isomers needs not to proceed *only* via unimolecular reactions induced by radiation; any conversion reaction including chemical reactions with enough abundant partners and without activation barriers could equally well operate on the right time-scales to fulfil the MEP in molecular clouds but not in hot cores. A thorough study of the potential energy surface of these three isomers, including the reaction paths connecting them, is called for in order to further progress in the understanding of this observational puzzle.

ACKNOWLEDGMENTS

We acknowledge financial support by MIUR under project CyberSar, call 1575/2004 of PON 2000–2006. We thank both referees for their useful comments and suggestions about significant literature on this subject which we had previously missed.

REFERENCES

Ahlrichs R., Furche F., Hättig C., Klopper W., Sierka M., Weigend F., 2007, TURBOMOLE, Version 5.9.1
Bauerschmitt R., Alrichs R., 1996, Chem. Phys. Lett., 256, 454
Becke A. D., 1988, Phys. Rev. A, 38, 3098
Belloche A., Menten K. M., Comito C., Müller H. S. P., Schilke P., Ott J., Thorwirth S., Hieret C., 2008, A&A, 492, 769
Beltrán M. T., Codella C., Viti S., Neri R., Cesaroni R., 2009, ApJ, 690, L93
Bennett C. J., Kaiser R. I., 2007, ApJ, 661, 899
Bockelée-Morvan D. et al., 2000, A&A, 353, 1101
Brown R. D., Crofts J. G., Godfrey P. D., Gardner F. F., Robinson B. J., Whiteoak J. B., 1975, ApJ, 197, L29
Cecchi-Pestellini C., Aiello S., 1992, MNRAS, 258, 125
Cecchi-Pestellini C., Ciaravella A., Micela G., 2006, A&A, 458, L13
Chengalur J. N., Kanekar N., 2003, A&A, 403, L43
Chyba C. F., Hand K. P., 2005, ARA&A, 43, 31
Crovisier J., 1994, J. Geophysical Res., 99, 3777
Crovisier J., Bockelée-Morvan D., Colom P., Biver N., Despois D., Lis D. C., the Team for target-of-opportunity radio observations of comets, 2004, A&A, 418, 1141
Despois D., Biver N., Bockelée-Morvan D., Crovisier J., 2005, in Lis D. C., Blake G. A., Herbst E., eds, Proc. IAU Symp. 231, Astrochemistry: Recent Successes and Current Challenges. Kluwer, Dordrecht, p. 469
Draine B. T., Bertoldi F., 1996, ApJ, 468, 269
Favata F., Flaccomio E., Reale F., Micela G., Sciortino S., Shang H., Stassun K. G., Feigelson E. D., 2005, ApJS, 160, 469
Gibb E., Nummelin A., Irvine W. M., Whittet D. C. B., Bergman P., 2000, ApJ, 545, 309
Gredel R., Lepp S., Dalgarno A., Herbst E., 1989, ApJ, 347, 289
Guinan E. F., Ribas I., 2002, in Montesinos B., Gimenez A., Guinan E. F., eds, ASP Conf. Ser. Vol. 269, The Evolving Sun and its Influence on Planetary Environments. Astron. Soc. Pac., San Francisco, p. 85
Halfen D. T., Apponi A. J., Woolf N., Polt R., Ziurys L. M., 2006, ApJ, 639, 237
Hartquist T. W., Williams D. A., eds, 1998, The Molecular Astrophysics of Stars and Galaxies. Clarendon Press, Oxford
Hollis J. M., Lovas F. J., Jewell P. R., 2000, ApJ, 540, L107
Hollis J. M., Vogel S. N., Snyder L. E., Jewell P. R., Lovas F. J., 2001, ApJ, 554, L81
Huebner W. F., Keady J. J., Lyon S. P., 1992, Ap&SS, 195, 1
Jones R. O., Gunnarsson O., 1989, Rev. Modern Phys., 61, 689
Karunanandan R., Hölscher D., Dillon T. J., Horowitz A., Crowley J. N., Vereecken L., Peeters J., 2007, J. Phys. Chem. A, 111, 897
Lattelais M., Pauzat F., Ellinger Y., Ceccarelli C., 2009, ApJ, 696, L133
Limão-Vieira P. et al., 2006, Chem. Phys., p. 339
Liu S.-Y., Mehringer D. M., Snyder L. E., 2001, ApJ, 552, 654
MacDonald G. H., Gibb A. G., Habing R. J., Millar T. J., 1996, A&AS, 119, 333
Marques M. A. L., Castro A., Bertsch G. F., Rubio A., 2003, Comput. Phys. Communications, 151, 60
Marques M. A. L., Gross E. K. U., 2004, Annu. Rev. Phys. Chem., 55, 427
Martin J. M. L., El-Yazal J., Francois J., 1996, J. Phys. Chem., 100, 15358
Mehringer D. M., Snyder L. E., Miao Y., Lovas F. J., 1997, ApJ, 480, L71
Miao Y., Snyder L. E., 1997, ApJ, 480, L67
Micela G., 2002, in Montesinos B., Gimenez A., Guinan E. F., eds, ASP Conf. Ser. Vol. 269, The Evolving Sun and its Influence on Planetary Environments. Astron. Soc. Pac., San Francisco, p. 107
Mulas G., 1998, A&A, 338, 243
Perdew J. P., 1986, Phys. Rev. B, 33, 8822
Prasad S. S., Tarafdar S. P., 1983, ApJ, 267, 603
Remijan A. J., Hollis J. M., 2006, ApJ, 640, 842
Remijan A., Snyder L. E., Liu S.-Y., Mehringer D., Kuan Y.-J., 2002, ApJ, 576, 264
Remijan A. J., Wyrowski F., Friedel D. N., Meier D. S., Snyder L. E., 2005, ApJ, 626, 233
Remijan A. J. et al., 2006, ApJ, 643, 567
Ribas I., Guinan E. F., Güdel M., Audard M., 2005, ApJ, 622, 680
Senent M. L., 2004, J. Phys. Chem. A, 108, 6286
Senent M. L., Villa M., Meléndez F. J., Domínguez-Gómez R., 2005, ApJ, 627, 567
Snyder L. E., 2006, Proc. Natl. Acad. Sci., 103, 12243
Stein S. E., Rabinovitch B. S., 1973, J. Chem. Phys., 58, 2438
Suto M., Wang X., Lee L. C., 1988, J. Phys. Chem., 92, 3764
Troullier N., Martins J. L., 1991, Phys. Rev. B, 43, 1993
Visser R., Geers V. C., Dullemond C. P., Augereau J., Pontoppidan K. M., van Dishoeck E. F., 2007, A&A, 466, 229
Wächtershäuser G., 2000, Sci, 289, 1307
Williams J. P., Blitz L., McKee C. F., 2000, in Mannings V., Boss A. P., Russell S. S., eds, Protostars and Planets IV. Univ. Arizona Press, Tucson, p. 97
Wilner D. J., De Pree C. G., Welch W. J., Goss W. M., 2001, ApJ, 550, L81
Yabana K., Bertsch G. F., 1999, Int. J. Quantum Chem., 75, 55

APPENDIX A

We performed all calculations in the framework of DFT, using the quantum chemistry packages TURBOMOLE (Ahlrichs et al. 2007) and OCTOPUS (Marques et al. 2003).

A1 Geometry optimizations

To find the electronic ground-state geometry of the three molecules considered, we first tested different combinations of density

functional and basis set exploiting TURBOMOLE to identify the most suitable one for our purposes. To this aim, we compared the experimental ground-state geometry of the acetic acid (Limão-Vieira et al. 2006) with the one we obtained using the combinations BP-SV(P), BP-TZVP, B3LYP-SV(P) and B3LYP-TZVP (see the TURBOMOLE manual[1] and references therein for precise definitions of basis sets and functionals). All combinations are in good agreement with experimental and previous theoretical data (Limão-Vieira et al. 2006), with the hybrid functional B3LYP showing a very slightly lower relative average error. This is not unexpected, since this functional is known to produce good results with other classes of organic molecules (e.g. Martin, El-Yazal & Francois 1996). Considering that both functionals show the same relative average error with both basis sets, we chose the larger TZVP basis set, since this is suggested by the TURBOMOLE manual as the default to get reliable quantitative results.

A2 Vibrational properties

For our modelling purposes, we calculated the harmonic vibrational frequencies of acetic acid, glycolaldehyde and methyl formate. All calculations were performed at the BP/TZVP level using the TURBOMOLE program package and resulted in being compatible with previously published results (Senent 2004; Senent et al. 2005; Limão-Vieira et al. 2006). The absolute intensities S of the IR-active modes are given in units of km mol^{-1}. For each vibrational mode of frequency $\tilde{\nu}$ expressed in cm^{-1}, the corresponding Einstein A coefficients for spontaneous emission can be computed as

$$A\,(\mathrm{s}^{-1}) = \frac{8\pi}{N_\mathrm{A} c}\,\tilde{\nu}^2\,S \simeq 1.2512\times10^{-7}\left(\frac{\tilde{\nu}}{\mathrm{cm}^{-1}}\right)^2\left(\frac{S}{\mathrm{km\,mol}^{-1}}\right)\frac{\mathrm{mol\,cm}^2}{\mathrm{km\,s}},$$

N_A being Avogadro's constant and c the velocity of light.

A3 Electronic spectra

In the real-time implementation of TD-DFT as given in OCTOPUS, the time-dependent Kohn–Sham equations are directly integrated in real time and the wavefunctions are represented by their discretized values on a spatial grid. The static Kohn–Sham wavefunctions are perturbed by an impulsive electric field and propagated for a given finite time interval. In this way, all of the frequencies of the system are excited. The whole absolute absorption cross-section $\sigma(E)$ then follows from the dynamical polarizability $\alpha(E)$, which is related to the Fourier transform of the time-dependent dipole moment of the molecule. The relation is

$$\sigma(E) = \frac{8\pi^2 E}{hc}\,\Im\{\alpha(E)\}, \tag{A1}$$

where h is Planck's constant, $\Im\{\alpha(E)\}$ is the imaginary part of the dynamical polarizability and c the velocity of light in vacuum.

We performed the OCTOPUS calculations using the Becke (1988) exchange and Perdew (1986) correlation functionals. The ionic potentials are replaced by norm-conserving pseudo-potentials (Troullier & Martins 1991). We used a grid spacing of 0.12 Å and a box size of 6.8 Å, determined by convergence tests on ground-state properties and on the photoabsorption spectrum at energies of

[1] www.turbomole.com

Table A1. Vertical electronic transitions (eV) and corresponding oscillator strengths of the three molecules considered, as computed at the BP/TZVP level using the TURBOMOLE program package.

Acetic acid		Glycolaldehyde		Methyl formate	
5.70	7.3(−4)	4.46	3.6(−5)	5.82	1.3(−3)
6.94	5.4(−2)	4.49	2.4(−2)	7.46	6.9(−2)
7.74	4.7(−3)	6.43	2.9(−4)	7.70	1.5(−3)
8.25	2.6(−3)	7.34	3.2(−3)	7.86	3.7(−3)
8.37	1.3(−1)	7.35	1.1(−2)	8.24	1.9(−1)
8.82	1.9(−4)	7.57	8.7(−2)	8.54	3.0(−2)
9.05	3.3(−3)	7.61	3.0(−2)	8.74	7.6(−2)
9.08	1.4(−4)	8.48	6.1(−2)	8.83	4.3(−3)
9.16	8.1(−4)	8.50	1.6(−2)	9.27	1.3(−4)
9.27	2.9(−3)	8.63	1.1(−3)	9.39	7.3(−4)
9.33	1.2(−1)	8.83	1.7(−2)	9.48	4.2(−5)
9.88	1.1(−1)	8.90	4.3(−2)	9.68	3.8(−2)
10.03	6.2(−4)	9.05	2.0(−1)	9.78	1.1(−2)
10.07	1.1(−1)	9.51	3.0(−2)	9.89	8.1(−2)
10.36	6.6(−4)	9.66	3.4(−4)	10.11	9.2(−2)
10.52	5.1(−3)	9.69	6.8(−3)	10.24	2.3(−2)
10.58	8.8(−2)	9.77	6.0(−2)	10.36	9.4(−4)
10.80	9.2(−2)	10.08	9.0(−3)	10.58	1.4(−2)
10.88	3.4(−2)	10.47	4.0(−4)	10.66	7.6(−3)
10.92	4.8(−2)	10.52	6.0(−3)	10.96	8.6(−3)
10.95	3.1(−2)	10.60	1.3(−3)	11.13	1.4(−2)
11.09	1.7(−3)	10.66	6.5(−2)	11.16	1.6(−3)
11.44	2.1(−2)	10.70	4.6(−3)	11.24	4.4(−4)
11.51	6.7(−2)	10.87	2.8(−3)	11.26	2.3(−2)
11.60	7.1(−3)	10.93	1.2(−1)	11.34	1.1(−2)
11.75	9.7(−3)	10.95	1.2(−3)	11.46	1.3(−2)
11.82	4.1(−6)	11.05	8.3(−4)	11.61	7.9(−2)
11.84	1.2(−1)	11.15	1.2(−1)	11.68	2.1(−2)
12.09	7.9(−2)	11.46	6.2(−2)	11.84	6.3(−2)
12.11	1.4(−3)	11.62	1.0(−2)	11.96	1.8(−1)
12.17	4.5(−2)	11.64	3.9(−3)	11.97	4.2(−3)
12.21	6.0(−4)	11.95	5.4(−2)	11.99	3.6(−2)
12.34	9.0(−3)	12.03	4.1(−2)	12.07	1.5(−2)
12.45	1.1(−2)	12.26	1.5(−3)	12.11	9.0(−3)
12.58	1.1(−1)	12.37	7.9(−4)	12.26	6.5(−3)
12.71	8.5(−2)	12.60	4.5(−2)	12.48	5.5(−2)
12.75	4.3(−2)	12.71	2.9(−2)	12.57	1.4(−1)
12.88	1.4(−2)	12.72	3.0(−3)	12.70	8.0(−3)
12.89	1.3(−2)	12.72	3.1(−2)	12.71	1.8(−4)
12.92	4.0(−2)	12.80	2.3(−3)	12.84	1.3(−1)
12.93	2.4(−2)	12.87	7.5(−3)	12.92	1.1(−2)
13.00	5.6(−3)	12.92	1.5(−2)	13.02	4.4(−3)
13.05	1.3(−1)	12.96	8.7(−2)	13.03	1.4(−1)
13.10	5.6(−2)	13.11	4.3(−2)	13.16	1.6(−1)
13.21	2.0(−1)	13.13	2.1(−1)	13.24	5.4(−2)
13.47	2.7(−2)	13.19	5.2(−2)	13.28	1.4(−2)
13.53	1.3(−2)	13.23	5.8(−2)	13.42	5.3(−2)
13.59	1.3(−1)	13.61	1.1(−2)	13.42	4.9(−2)
13.66	4.4(−2)	13.68	3.9(−2)	13.61	1.0(−2)
13.76	7.9(−2)	13.72	2.8(−2)	13.66	1.4(−1)
13.77	2.9(−4)	13.83	1.7(−2)	13.74	5.8(−2)
14.10	6.4(−3)	13.89	2.4(−2)	13.83	2.1(−2)
14.22	4.0(−2)	13.94	7.8(−2)	13.91	3.3(−2)
14.23	6.0(−3)	14.00	2.8(−2)	14.02	2.9(−2)
14.25	9.8(−3)	14.02	4.1(−2)	14.06	3.2(−3)
14.41	2.2(−4)	14.07	1.4(−2)	14.14	6.3(−3)
14.50	5.1(−3)	14.17	5.2(−2)	14.23	5.1(−2)
14.62	3.2(−2)	14.24	5.1(−3)	14.28	2.3(−2)
14.65	6.2(−2)	14.39	2.0(−1)	14.29	5.1(−2)
14.68	9.2(−3)	14.47	4.0(−2)	14.52	8.5(−3)

$\lesssim$10 eV. This box size ensures that each atom is at least 4 Å away from its edges. We furthermore added a 1 Å thick absorbing boundary, which partially quenches spurious resonances due to standing waves in the finite simulation box used to confine the molecules (Yabana & Bertsch 1999; Marques et al. 2003). We used a total time integration length $T = 20\,\hbar$/eV, corresponding to an energy resolution of $\hbar/T = 0.05$ eV. For the numerical integration of the time evolution, we used a time step of 0.0008 $\hbar$/eV, which ensured energy conservation with good accuracy, within numerical noise.

In the most widely used frequency-space TD-DFT implementation, the poles of the linear response function correspond to vertical excitation energies and the pole strengths to the corresponding oscillator strengths. With this method, computational costs scale steeply with the number of required transitions and electronic excitations are thus usually limited to the low-energy part of the spectrum. The frequency-space TD-DFT calculations with TURBOMOLE were performed at the BP/TZVP level of theory, since this showed the best agreement with experimental data. In Table A1, we report the first 60 singlet–singlet electronic transitions of the three molecules under study with the corresponding oscillator strengths.

This paper has been typeset from a TEX/LATEX file prepared by the author.